Review Article | Cardiovascular Imaging

http://dx.doi.org/10.3348/kjr.2016.17.4.445
pISSN 1229-6929 · eISSN 2005-8330
Korean J Radiol 2016;17(4):445-462

Korean Journal of Radiology
KJR

Hemodynamic Measurement Using Four-Dimensional Phase-Contrast MRI: Quantification of Hemodynamic Parameters and Clinical Applications

Hojin Ha, PhD[1], Guk Bae Kim, PhD[2], Jihoon Kweon, PhD[3], Sang Joon Lee, PhD[1, 4], Young-Hak Kim, MD, PhD[3], Deok Hee Lee, MD, PhD[5], Dong Hyun Yang, MD, PhD[5], Namkug Kim, PhD[5, 6]

[1]POSTECH Biotech Center and [4]Department of Mechanical Engineering, Pohang University of Science and Technology, Pohang 37673, Korea; [2]Asan Institute of Life Science, Departments of [3]Cardiology, [5]Radiology, and [6]Convergence Medicine, Asan Medical Center, University of Ulsan College of Medicine, Seoul 05505, Korea

Recent improvements have been made to the use of time-resolved, three-dimensional phase-contrast (PC) magnetic resonance imaging (MRI), which is also named four-dimensional (4D) PC-MRI or 4D flow MRI, in the investigation of spatial and temporal variations in hemodynamic features in cardiovascular blood flow. The present article reviews the principle and analytical procedures of 4D PC-MRI. Various fluid dynamic biomarkers for possible clinical usage are also described, including wall shear stress, turbulent kinetic energy, and relative pressure. Lastly, this article provides an overview of the clinical applications of 4D PC-MRI in various cardiovascular regions.

Index terms: *4D phase-contrast MRI; 4D flow MRI; Blood flow; Hemodynamics*

INTRODUCTION

Quantification of the hemodynamic features of blood flow is important because these features are closely related to the development of cardiovascular diseases. Blood flow exerts various types of fluid dynamic forces on the blood vessel, including pressure force and frictional shearing stress. Endothelial cells on the vessel wall sense and respond to these hemodynamic conditions by adapting their morphology and proliferation (1). The pathological hemodynamic forces exerted on the vessel wall consequently induce inflammatory lesions in the vessel that promote the development of atherosclerosis, aortic dilatation, and aortic aneurysm (2-5). In addition, the mechanical forces of the blood flow influence plaque vulnerability and the risk of aneurysm rupture (6, 7). Therefore, quantification and understanding of the characteristics of blood flow are important in diagnosing and predicting the future risk of cardiovascular disease.

Time-resolved, three-dimensional (3D) phase-contrast (PC) magnetic resonance imaging (MRI), which is also termed four-dimensional (4D) PC-MRI or 4D flow MRI, was recently developed to investigate spatial and temporal variations in the hemodynamic features of blood flow (8,

Received January 20, 2016; accepted after revision April 22, 2016.
This research was partially supported by a grant of the Korea Health Technology R&D Project through the Korea Health Industry Development Institute (KHIDI), funded by the Ministry of Health & Welfare, Republic of Korea (HI12C0630) and the National Research Foundation of Korea (NRF) grant funded by the Korea government (MSIP) (NRF-2015R1A2A2A04003034).
Corresponding author: Namkug Kim, PhD, Department of Convergence Medicine, University of Ulsan College of Medicine, Asan Medical Center, 88 Olympic-ro 43-gil, Songpa-gu, Seoul 05505, Korea.
• Tel: (822) 3010-6573 • Fax: (822) 3010-6196
• E-mail: namkugkim@gmail.com and;
Dong Hyun Yang, MD, PhD, Department of Radiology, Asan Medical Center, University of Ulsan College of Medicine, 88 Olympic-ro 43-gil, Songpa-gu, Seoul 05505, Korea.
• Tel: (822) 3010-5820 • Fax: (822) 3010-6196
• E-mail: donghyunyang@gmail.com

9). This technique permits the volumetric assessment of blood flow in the entire vasculature of interest and enables the volumetric quantification and retrospective analysis of blood flow in any arbitrary angle, which is not possible with conventional two-dimensional (2D) PC-MRI.

Based on the volumetric velocity data of 4D PC-MRI, various methods have been developed to visualize and quantify blood flow, and their clinical implications have been studied (10). The visualization of 4D PC-MRI data using vector field, streamline, pathline, isosurface, and volume rendering has been effective in identifying the abnormal alteration of blood flow in various vessels, such as the aorta, carotid arteries, and cerebral vessels (11-13). Volumetric acquisition of the blood flow also enables better visualization and quantification of the complex nature of intracardiac blood flow (14, 15). 4D PC-MRI provides not only the conventional flow quantifications, but also various fluid dynamic biomarkers with potential clinical utility, such as wall shear stress (WSS) (3, 4), turbulent kinetic energy (TKE) (16-18), vorticity (19, 20), pressure gradient (21-23), and pulse wave velocity (24, 25).

The purpose of our present review is to discuss recent advances in 4D PC-MRI. We briefly overview the principles and analytical procedures of 4D PC-MRI, and introduce various fluid dynamic biomarkers that can be obtained using the technique. In addition, we overview the clinical applications of 4D PC-MRI in various cardiovascular regions. Finally, we describe the limitations and potential of the technique.

Principles and Methodology

Imaging Principles

Phase-contrast MRI is based on variations in the Larmor precession frequency under a magnetic field. The Larmor precession frequency ω_L of spins under a magnetic gradient can be described as:

$$\omega_L(\vec{r}, t) = \gamma B_0 + \gamma \Delta B_0 + \gamma \vec{r}(t)\vec{G}(t) \quad (1)$$

where γ is the gyromagnetic ratio, $\vec{r}$ is the displacement, B_0 is the static magnetic field, ΔB_0 is the local field inhomogeneity, and $\vec{G}$ is the magnetic field gradient. Assuming that the fluid velocity $\vec{v}$ is constant during the acquisition, the displacement $\vec{r}$ can be described as $\vec{r}(t) = \vec{r_0} + \vec{v}(t - t_0)$, where t_0 is the excitation time and $\vec{r_0}$ is the displacement at t_0. Then, the phase shift of the fluid with the velocity $\vec{v}$ under the magnetic gradient can be obtained by integrating the ω_L from t_0 to the echo time (TE) as:

$$\begin{aligned}\phi(\vec{r}, TE) &= \phi_0 + \gamma\vec{r_0}\int_{t_0}^{TE}\vec{G}(t)dt + \gamma\vec{v}\int_{t_0}^{TE}\vec{G}(t)tdt + \ldots \\ &= \phi_0 + \gamma\vec{r_0}M_0 + \gamma\vec{v}M_1 + \ldots\end{aligned} \quad (2)$$

Here, the first term on the right-hand side (ϕ_0) is the background phase offset which is influenced by the field inhomogeneity. The second and third are the phase accumulations from the stationary and moving spins, respectively, under the magnetic gradient $\vec{G}$. The integral terms describing the influence of the magnetic gradient on the static and moving spins are named the zeroth and the first gradient moments, M_0 and M_1, respectively.

Conventional 2D PC-MRI uses a bipolar gradient along the flow-encoding direction before the readout sequence (Fig. 1). The bipolar gradient removes the phase accumulations from the stationary spins, which results in only the background phase offset and the flow-related phase accumulations (the first and third terms in Eq. 2). The PC-MRI sequence typically uses two acquisitions with different M_1 values to remove the unknown phase offset. In 2D PC-MRI, two acquisition schemes are conventionally used. The first type of the acquisition scheme employs the flow-compensation gradient with the flow-encoding gradient to obtain the reference image. The second type of the acquisition employs the combination of the flow-encoding gradient and the following gradient with the opposite polarity. Meanwhile, the no bipolar gradient for the reference image is rarely used. In 4D PC-MRI, the first acquisition scheme is mostly used, and the reference acquisition without the bipolar gradient is rarely used.

The phase difference between the two scans is directly related to the velocity of the flow as follows:

$$\Delta\phi = \gamma\vec{v}\Delta M_1 \quad (3)$$

The velocity-encoding parameter, which is named V_{enc} or VENC, determines the maximum velocity by changing the difference in the first gradient momentum ΔM_1 as follows:

$$VENC = \frac{\pi}{\gamma\Delta M_1} \quad (4)$$

$$v = VENC\frac{\Delta\phi}{\pi} \quad (5)$$

Here, it can be noted that the flow velocity that is as

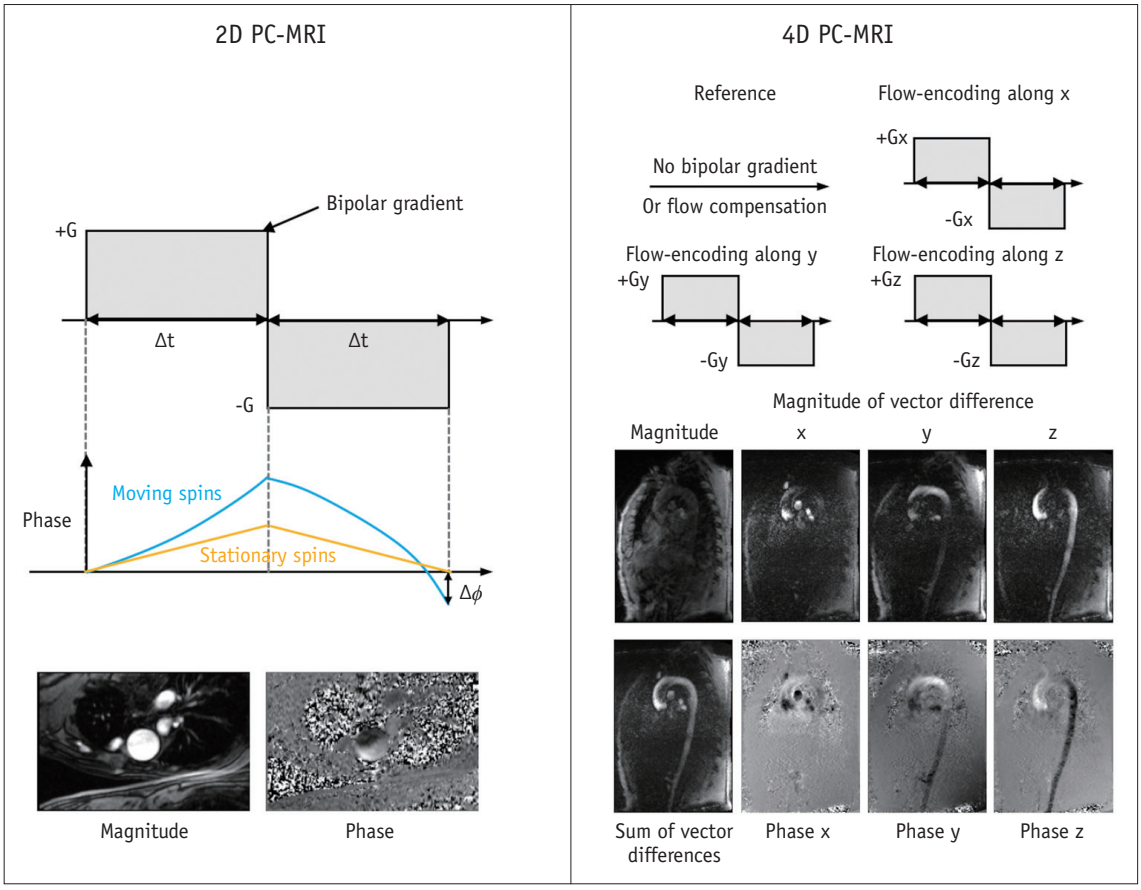

Fig. 1. Principles of 2D PC-MRI and 4D PC-MRI. Conventional PC-MRI uses bipolar gradient along flow-encoding direction before readout sequence. Bipolar gradient removes phase accumulations from stationary spins, which results in only background phase offset and flow-related phase accumulations. PC-MRI sequence typically uses two acquisitions with different M_1 values to remove unknown phase offset. PC = phase-contrast, 2D = two-dimensional, 4D = four-dimensional

high as the pre-determined VENC (cm/s) gives the phase shift of π.

In contrast to conventional 2D PC-MRI with two acquisitions, 4D PC-MRI usually uses four-point scans by measuring the three-directional velocity encodings and one-flow compensation encoding, as shown in Figure 1 (26). Assuming the background phase offset is the same in the four different scans, the three-directional velocities can be obtained by substituting the phase shifts in the three-directional encodings with the phase in the reference image.

4D PC-MRI usually exports three-directional volumetric phase images for velocity reconstruction, one volumetric magnitude image, and four volumetric vector difference images (three-directional images and one summation image) for depicting vascular anatomic information (27, 28). The exported images vary according to the vendor and sequence of the MRI scanner.

Image Acquisition and Analysis Procedures

Scan Parameters

When a patient is registered for 4D PC-MRI, adequate scan parameters need to be used to obtain data of sufficient quality with a reasonable scan time. Of the various scan parameters, the most important parameters include field of view, spatial resolution, temporal resolution, and the VENC (Fig. 2). The field of view would ideally encompass the entire vasculature, but a larger field of view requires a greater amount of scan data and, consequently, a longer scan time. Therefore, the field of view should be confined to the smallest region that contains the region of interest, in order to reduce the scan time.

The spatial resolution should also be as high as possible because a higher spatial resolution results in more accurate flow quantification and helps to identify smaller-scaled flow phenomena (29). However, the smaller the voxel, the longer the scan time and the lower the signal-to-noise ratio (SNR).

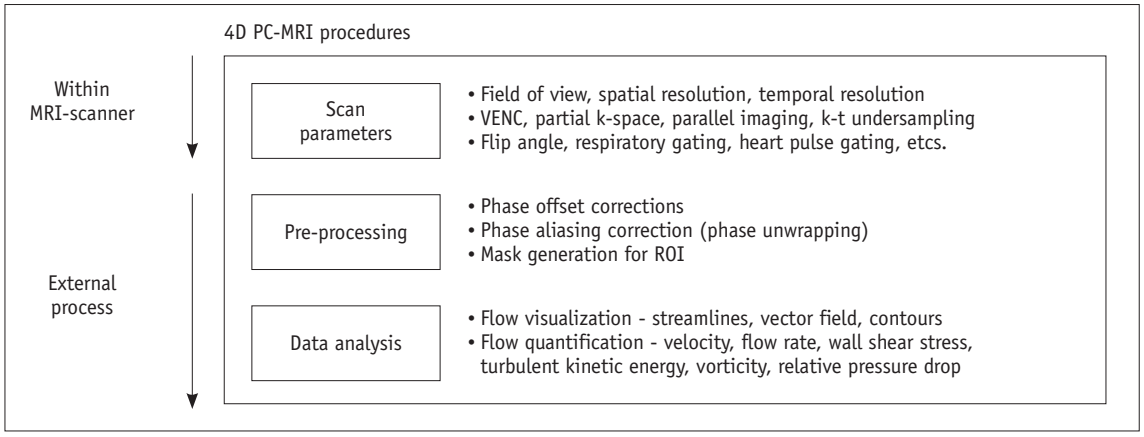

Fig. 2. Procedures for 4D PC-MRI. Image quality of raw data can be influenced by adequate scan parameters including field of view, spatial resolution, temporal resolution, and VENC. In addition, appropriate pre-processing and data analysis techniques are also important for accurate quantification of hemodynamic features. PC = phase-contrast, ROI = region of interest, 4D = four-dimensional

Therefore, a compromise between the spatial resolution, scan time, and SNR is needed for scanning. Practically, voxel sizes of 2.5–3.0 mm and 0.7–1.5 mm are usually used to measure cardiac blood flow and intracranial blood flow, respectively (30-35).

Temporal resolution should also be as short as possible to accurately identify temporal variations in pulsating blood flow. However, in 4D PC-MRI, the number of MRI signal acquisitions is directly proportional to the number of cardiac phases, which is the number of temporal steps of the data for describing the whole pulsatile cycle. Therefore, the temporal resolution is limited to reduce the total scan time. Typically, a temporal resolution of around 40 ms is usually used to measure pulsatile aorta flow (31, 35).

As described in Imaging Principles section, the VENC determines the maximum encoding velocity of the blood flow. Because a flow velocity higher than the pre-determined VENC will result in phase aliasing, the VENC should be higher than the expected maximum velocity of the flow. However, because a higher VENC will also decrease the velocity-to-noise ratio, a VENC around 10% higher than the expected maximum velocity flow is usually recommended (30).

In addition to the parameters described above, various other parameters, including partial k-space coverage, parallel imaging, and k-t undersampling, also need to be considered to limit the scan time and improve the SNR of the data. For a more detailed description of the scan parameters, readers should refer to previous reviews of 4D PC-MRI (10, 30).

Pre-Processing

Even though 4D PC-MRI scanning exports various types of reconstructed images, as described in Imaging Principles section, the phase image from the 4D PC-MRI is preferred for further processing, such as flow quantification and analysis. However, the phase image includes various types of inherent errors. Therefore, pre-processing of the raw data is required.

The phase image from the PC-MRI sequence has phase offset errors from the concomitant gradient (or Maxwell terms) (36), gradient field non-linearity (37), and eddy currents (38). The existence of these background phase errors should be understood, and the corresponding correction schemes are required for phase correction. Commercial analysis software for 4D PC-MRI, such as 4D Flow (Siemens, Munich, Germany), GT-Flow (Gyrotools LLC, Winterthur, Switzerland), CAAS MR 4D Flow (Pie Medical Imaging BV, AJ Maastricht, the Netherlands), and Arterys (Arterys, San Francisco, CA, USA), provides phase correction schemes. However, to adjust the correction schemes to their own data, most researchers continue to use their own correction schemes based on MATLAB (Natick, MA, USA) or other programming languages.

If the flow velocity is higher than the pre-determined VENC, the raw data will contain phase aliasing or phase wrapping. If the flow quantification is processed without considering the phase aliasing, the results will be severely corrupted by the phase aliasing. Therefore, if such phase aliasing is unavoidable, a phase-unwrapping algorithm is needed to recover the information from regions of phase aliasing. However, a generalized algorithm for phase unwrapping has not been derived yet, and each

Korean Journal of Radiology
KJR

algorithm may have different performances according to the characteristics of the phase data. Therefore, several studies have been performed to determine phase-unwrapping algorithms and compare the performances of various algorithms (39-44).

Once the raw data have been appropriately corrected, the next step is image segmentation to generate masking images to distinguish the fluid region and the external static tissues in the phase images. Because the sum of vector difference image (Fig. 1), named the complex difference image, can clearly distinguish the flow and the surrounding region, this image is usually used as an angiogram for identifying arteries and veins from the static surrounding tissues (27, 28). If the sum of vector difference image does not have enough contrast between the fluid and static tissues due to a slow flow, a separate 3D MR angiography scan can also be used for registration. To generate the mask images from the angiograms, various types of segmentation schemes can be used, from manual segmentation based on pre-knowledge of the anatomy of interest to fully automatic mask generation (45-47).

Data Analysis

To analyze and visualize hemodynamic features using 4D PC-MRI, two approaches are available. The first option is to use commercial analysis tools for 4D PC-MRI. The commercial tools described in Pre-Processing section can be easily used to visualize and quantify the results. However, the commercial tools still provide only a limited number of basic flow parameters such as flow rates and volumes. Accordingly, most researchers calculate their own parameters based on their own platforms using MATLAB or other programming languages, and then visualize and analyze their data using conventional post-processing tools that are popular in the field of fluid dynamics, such as Tecplot (Tecplot, Bellevue, WA, USA) and Ensight (CEI, Apex, NC, USA).

The visualization of 4D PC-MRI data usually uses vector field, streamline and pathline (Figs. 3-8). A velocity vector field is a collection of velocity vectors in space (Fig. 3). It visualizes the speed and direction of the blood flow with a collection of arrows with a given magnitude and direction. Streamline is defined as a collection of curves that are

Table 1. Summary of Hemodynamic Parameters and Their Clinical Applications

Parameter*	Definition	Physiological Implication	Application in Previous Studies	Notes
Flow velocity & flow rate	Amount of blood transported	Abnormal increase or decrease in blood flow indicates possible ischemia or local contraction of vessel	1. Peak velocity at aortic valve (14, 68) 2. In- and outflow within intracardiac chamber (30, 56, 69, 70) 3. Flow rate through intracardiac branches (72, 73)	Sufficient spatial and temporal resolutions are required
WSS	Frictional shearing force on vessel	Abnormal alteration of flow pattern near vessel wall influences vascular dysfunction	1. WSS increase in patients with BAV (3, 4, 74) 2. Low & oscillatory WSS in carotid artery (2) 3. WSS increase in intracranial aneurysms (75-77)	WSS can be influenced by spatial resolution
Vortex	Rotational structure of blood flow	Abnormal appearance of vortical flow indicates abnormal alteration of flow pattern	1. Development of vortex flow at pulmonary hypertension (57)	Vortex identification can be highly influenced by noise
TKE	Turbulent kinetic energy	Increased TKE indicates more energy loss of blood flow	1. Increased TKE at aortic stenosis (17) 2. Increased TKE at cardiomyopathy (78)	More than two acquisitions are required
Relative pressure	Pressure gradient from arbitrary reference	Increased pressure drop indicates decreased blood flow or increased work load of heart	1. Pressure gradient through stenosis in aorta (23, 65, 66, 79, 80) and carotid, iliac (82), and renal (81) arteries 2. Pressure distribution at intracardiac plaque (83)	Influence of turbulence on pressure field cannot be included

*Note that most of parameters except flow velocity and flow rate are currently unavailable in most commercial software. Therefore, development of in-house software is required to estimate hemodynamic parameters. BAV = bicuspid aortic valve, TKE = turbulent kinetic energy, WSS = wall shear stress

tangent to the velocity vector of the flow at the specified time (Fig. 3). It resultantly indicates the direction of fluid element at the specified time point. On the other hand, the pathline is a collection of the trajectories that an individual fluid element flows over a certain time (Fig. 8). As a result, it indicates how each fluid element moves during the cardiac cycle.

Hemodynamic Quantification

While 4D PC-MRI provides the same basic flow quantifications as conventional 2D PC-MRI, the multidimensional data of 4D PC-MRI has facilitated the development of various fluid dynamic biomarkers for better assessing blood flow *in vivo*. The following sections introduce the principles and physiological meanings of the hemodynamic parameters that can be obtained using 4D PC-MRI (Table 1). However, most commercial software does not cover all of these quantifications. Therefore, the development of in-house software is required for these quantifications.

Velocity and Flow Rate

The velocity and flow rate of blood flow are the most basic fluid dynamic parameters used to compare the normal and pathological conditions of blood flow against baseline. A decreased local flow rate directly indicates the loss of blood being transported toward the corresponding tissue regions, which could be the result of local ischemia (48). A local increase in the blood velocity at stenotic regions, such as regions with aortic valve stenosis or aortic coarctation, is related to the severity of the stenosis (49, 50). Because 4D PC-MRI provides whole velocity data within the volume of interest, it is useful for quantifying the flow rate distribution of complex vessel networks and estimating the peak velocity within certain regions.

The velocity of the blood flow calculated from the 4D PC-MRI data is usually visualized using pathlines and streamlines with velocity color mapping (Fig. 3). For any arbitrary cross-sectional plane within the volumetric data, retrospective quantification of the flow rate can be carried out by integrating the velocity inside the specified lumen. Previous studies found that the velocity and flow rate from 4D PC-MRI were well correlated with those from 2D PC-MRI (51). Practically, around three voxels along the vessel diameter (around five voxels across the lumen area) were sufficient to accurately quantify the flow rate (29). However, the accuracy of the flow rate quantification using 4D PC-MRI can be at least somewhat influenced by the segmentation of the vessel because 4D PC-MRI generally has lower spatial resolution than 2D PC-MRI. Therefore, the accurate segmentation of the geometrical boundary of the vessel is important when assessing flow rate on 4D PC-MRI.

Wall Shear Stress

Wall shear stress is the frictional shearing stress exerted

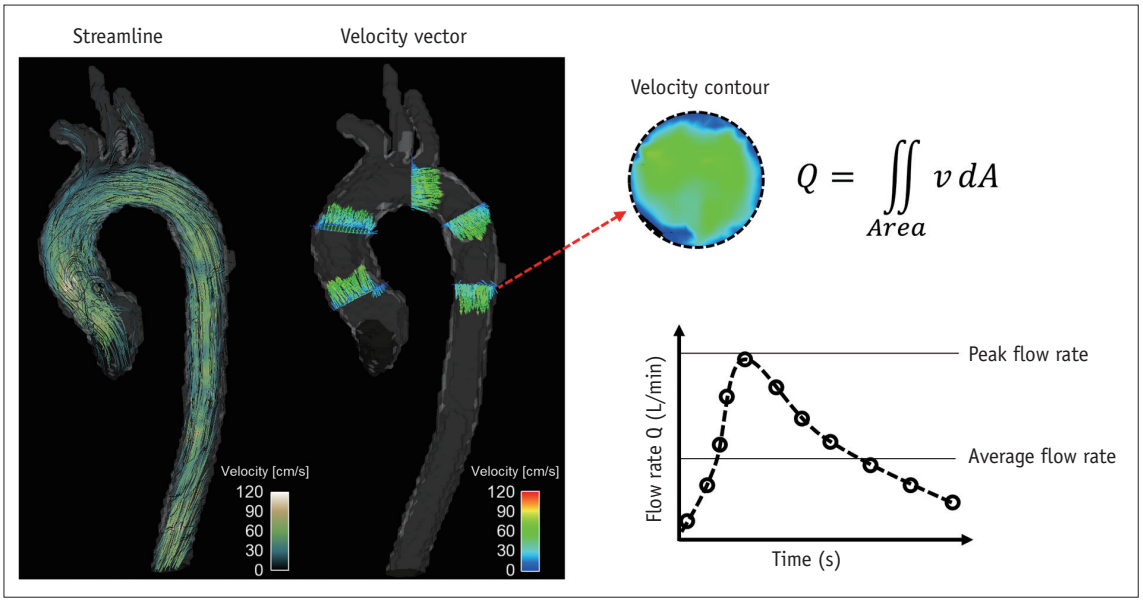

Fig. 3. Velocity visualization and quantification of flow rate. Streamline and velocity vector (left panel) can be used to visualize blood flow pattern in aorta. Spatial and temporal variation of blood flow can also be quantified by integrating four-dimensional velocity field data (right panel).

Korean Journal of Radiology
KJR

by fluid on the vascular wall. Recently, WSS distribution in arterial blood flow has received considerable attention because it has been associated with vascular diseases, specifically, atherosclerosis and aortic dilatation (2-4). By definition, WSS can be obtained by multiplying the viscosity of the fluid by the local velocity gradient at the wall as follows:

$$\tau = \mu \left. \frac{\partial u}{\partial n} \right|_{wall} \quad (6)$$

where τ is the WSS, n is the local wall normal displacement vector, u is the local velocity component, and μ is the dynamic viscosity. The unit of WSS is Pa or N/m^2 when the units of u, n, and μ are m/s, m, and $N \cdot s/m^2$, respectively.

The first step for WSS estimation is to obtain a smooth spline contour or surface of the lumen from the magnitude, phase, or mask images, so that the wall location and normal displacement vector can be estimated from the lumen contour or surface (Fig. 4). Then, the velocity near the wall along the normal vector is obtained by interpolating the neighboring velocity data, and the velocity gradient at the wall is calculated on the vessel lumen using the spline interpolation model, which provides the analytical derivative of the flow velocity (52). Consequently, WSS can be obtained by multiplying the obtained velocity gradient by the blood viscosity by assuming that the blood viscosity

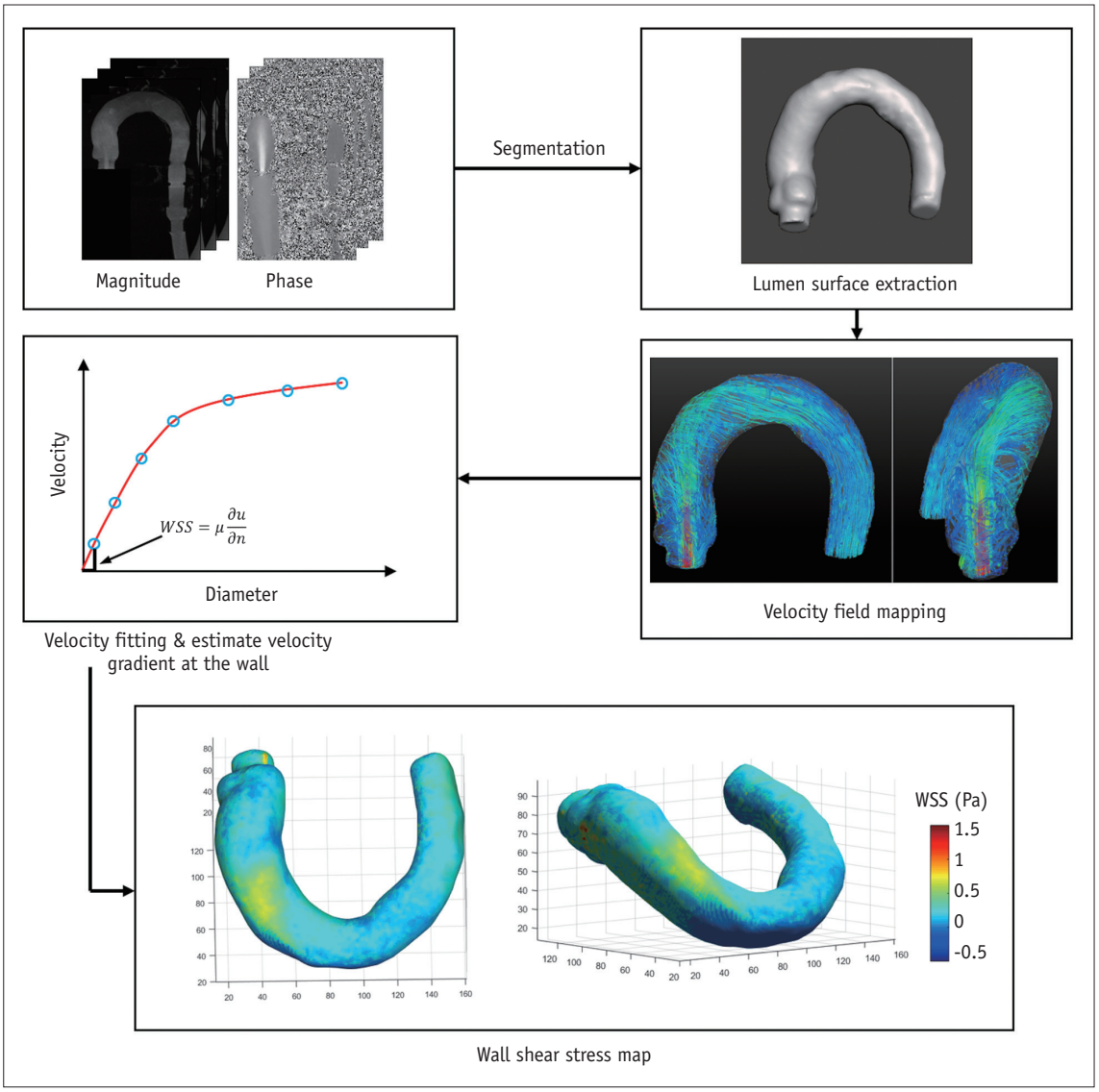

Fig. 4. Wall shear stress (WSS) estimation using 4D PC-MRI. First step for WSS estimation is to obtain smooth spline contour or surface of lumen from magnitude, phase, or mask images, so that wall location and normal displacement vector can be estimated from lumen contour or surface. WSS can be obtained by multiplying velocity gradient and blood viscosity. PC = phase-contrast, 4D = four-dimensional

is constant at around 4 centipoise (cP) (52). Finally, the obtained WSS is usually visualized using color-mapped surface rendering to distinguish the low and high WSS regions, and is quantified with segmentation (Fig. 4).

Turbulent Kinetic Energy

While the blood flow mostly comprises laminar flow, under certain conditions blood flow can be turbulent with high-velocity fluctuations. In particular, arterial blood flows with local contractions due to aortic valves, aortic coarctation, and atherosclerosis, usually develop a local turbulent blood flow (17, 18). Quantification of the turbulent velocity fluctuation is important because it increases the pressure drop along the vessel by elevating the fluid energy dissipation, which consequently results in a requirement for more energy to maintain the perfusion of the blood flow (53). In addition, a higher turbulence of the flow than baseline under similar flow rate conditions also indicates more severe stenosis (17).

Previously, Dyverfeldt et al. (16) derived an equation for TKE estimation based on the relationship between the intravoxel velocity distribution and the MR signal from a standard PC-MRI scan (Fig. 5). This estimation assumes that the spin velocities within a voxel are normally distributed in turbulent flow. Three-directional standard deviation components of the turbulent flow can be obtained from the magnitude images of the four-point scans as follows (54):

$$\sigma_i = \frac{1}{k_v}\sqrt{2\ln\left(\frac{|S_0|}{|S_i|}\right)} \quad (7)$$

where σ_i indicates the standard deviation in the ith-direction (x, y, z), k_v indicates the net motion sensitivity ($k_v = \pi / VENC$), and $|S_0|$ and $|S_i|$ indicate the magnitude of the MRI signal obtained without and with flow sensitivity, respectively. The TKE per unit volume can be estimated from σ as follows:

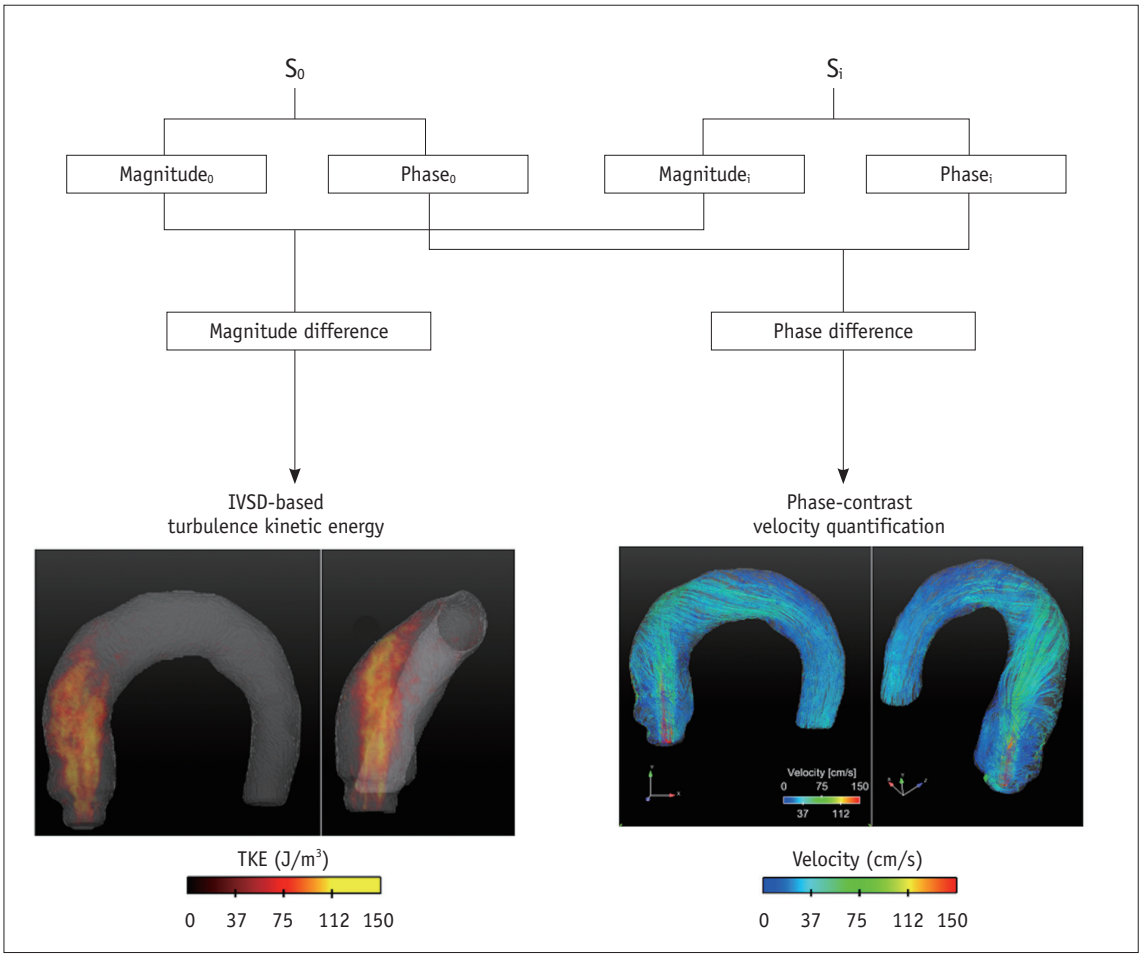

Fig. 5. Principle of TKE estimation. TKE estimation is based on relationship between intravoxel velocity distribution and MR signal from standard PC-MRI scan. Therefore, TKE can be quantified from quantification of magnitude difference under velocity gradient. IVSD = intra-voxel standard deviation, PC = phase-contrast, TKE = turbulent kinetic energy

Korean Journal of Radiology
KJR

$$TKE = \frac{1}{2}\rho\sum_{i=1}^{3}\sigma_i^2 \quad [J / m^3] \tag{8}$$

where ρ is the fluid density and σ_i indicates the standard deviation in the ith-direction (x, y, z).

Importantly, the sensitivity of TKE estimation is influenced by the VENC (or k_v). The sensitivity of the TKE estimation is optimal when the signal magnitude ratio $|S|/|S_0|$ becomes approximately 0.6 (analytically: $e^{-1/2}$) (16). However, the VENC value for obtaining $|S|/|S_0|$–0.6 is usually less than the maximum velocity of the flow; consequently, the scan for TKE estimation usually results in phase aliasing. Therefore, at least two acquisitions with different VENC values are generally requested to obtain both the velocity field and TKE distribution.

Vortical Structure

Blood flow frequently generates vortical flow patterns (e.g., locally rotational or helical flows) in various cardiovascular regions, including the left ventricle, ascending aorta, and pulmonary vessel (55-57). While the in-depth relationship between the vortical flow and the pathology is not yet fully understood, the existence and intensity of the vortical flow are influenced by pathological conditions, such as aortic aneurysm, pulmonary hypertension, and heart disease (55-57). Therefore, accurate quantification of the vortical flow structure is important in revealing the relationship between vortical flow structures and vascular diseases, and to develop a fluid dynamic index based on the vortical flow structure.

Vorticity

One of the basic fluid dynamic parameters describing the rotational motion of the fluid element is the vorticity vector of the flow. Vorticity $\vec{\omega}$ is defined as the curl of the velocity vector $\vec{v}$:

$$\vec{\omega} = \nabla \times \vec{v} = \left(\frac{\partial v_z}{\partial_y} - \frac{\partial v_y}{\partial_z}, \frac{\partial v_x}{\partial_z} - \frac{\partial v_z}{\partial_x}, \frac{\partial v_y}{\partial_x} - \frac{\partial v_x}{\partial_y}\right) \tag{9}$$

where ∇ is the del operator. Here, each vorticity component indicates the swirling intensity of the fluid element along the corresponding axis (Fig. 6A). The unit of vorticity is s^{-1}.

λ_2-Criterion

The λ_2-criterion is the one of the most popular methods for identifying the vortical flow structure (58). This algorithm is based on the velocity gradient tensor J, where $J \equiv \nabla\vec{v}$. Then, the velocity gradient tensor can be decomposed into the symmetric S and asymmetric Ω terms as follows:

$$S = \frac{J + J^T}{2},\ \omega = \frac{J - J^T}{2} \tag{10}$$

where T indicates the transpose of the matrix. Identification of the eigenvalues of $S^2 + \Omega^2$ for each voxel results in three eigenvalues, λ_1, λ_2, and λ_3, where $\lambda_1 \geq \lambda_2 \geq \lambda_3$. Finally, the vortex flow region can be found where λ_2 is negative. Since this algorithm is Galilean invariant, the vortical flow structures can be identified even though the vortical flow is overlaid with the uniform translational velocity field.

Critical Point Analysis

Critical point analysis is also a vortex structure identification method based on critical point analysis of the local velocity gradient tensor and its corresponding eigenvalues (59, 60). The eigenvalues of the local velocity

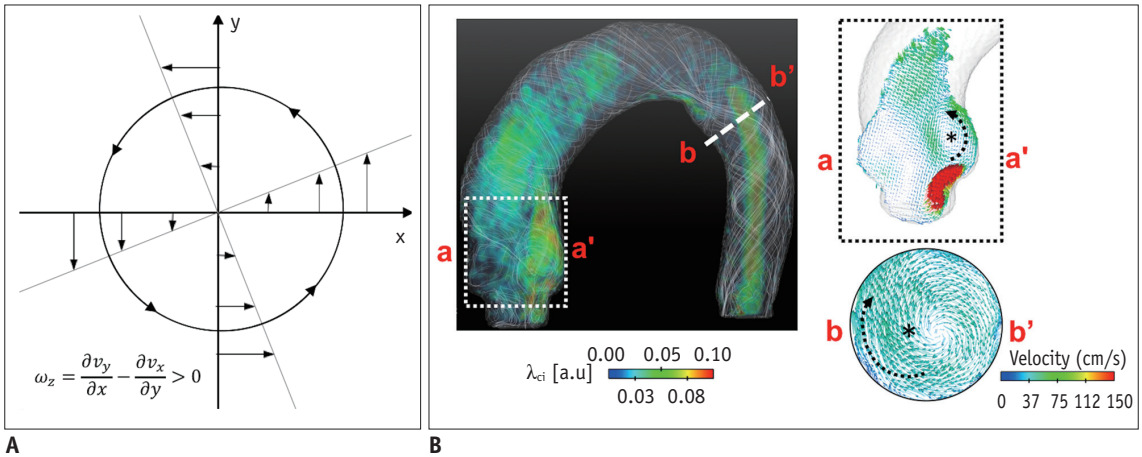

Fig. 6. Identification of vortical flow pattern.
A. Vorticity in rotational flow. **B.** λ_{ci} quantification in aortic flow. Note that vortical flow structures induce high vorticity and λ_{ci}.

gradient tensor J have one real eigenvalue (λ_r) and a pair of complex conjugate eigenvalues ($\lambda_{cr} \pm i\lambda_{ci}$) when the discriminant of its characteristic equation is positive. Then, λ_{ci}^{-1} represents the period required for a fluid particle to rotate along the λ_{cr} axis (61). Therefore, the region with nonzero λ_{ci} corresponds to the local vortical flow, and the magnitude of λ_{ci} is related to the intensity of the vortical flow. This method is also Galilean invariant and contains information on the strength of the vortical flow, in contrast to the λ_2-criterion (Fig. 6B).

Non-Invasive Estimation of Pressure Drop

A blood flow pressure loss indicates the loss of flow energy generated from the heart. An increase in the energy loss results in decreased blood flow or an increased workload on the heart for maintaining the same flow rate. Therefore, the pressure gradient is widely used as an important biomarker of stenosis severity, such as that caused by aortic valve stenosis or aortic coarctation (62, 63).

Application of a pressure catheter has been a gold standard method for measuring the pressure values *in vivo*. However, it is not preferred due to its invasiveness. Alternatively, the pressure gradient can be estimated by Doppler echocardiography, which is a non-invasive method for measuring the maximum velocity of the flow across the stenosis region and estimating the pressure gradient based on a simplified Bernoulli equation (64). However, this method does not provide the spatial and temporal variations in the pressure. In addition, the accuracy of the results can vary according to the flow conditions because the simplified Bernoulli equation assumes the flow is laminar without turbulence, and it also neglects the viscous energy dissipation (65).

Recently, relative pressure estimation using 4D PC-MRI has been introduced as an alternative method for estimating the pressure loss of the blood flow across the aorta and stenosis (23, 65, 66). The method aims to calculate the pressure gradient at each voxel from the Navier-Stokes equation and reconstruct the pressure field over the entire vessel of interest (Fig. 7). Assuming that blood is a viscous, incompressible fluid, the Navier-Stokes equation can be arranged as follows:

$$-\nabla p = \rho\left(\frac{\partial v}{\partial t} + v\cdot\nabla v\right) - \mu\nabla^2 v \quad (11)$$

where p is the pressure, μ is the viscosity, ρ is the density, and v is the velocity. Here, the gravitational term has been neglected. Because the temporal variations in the 3D velocity can be obtained from 4D PC-MRI, the spatial

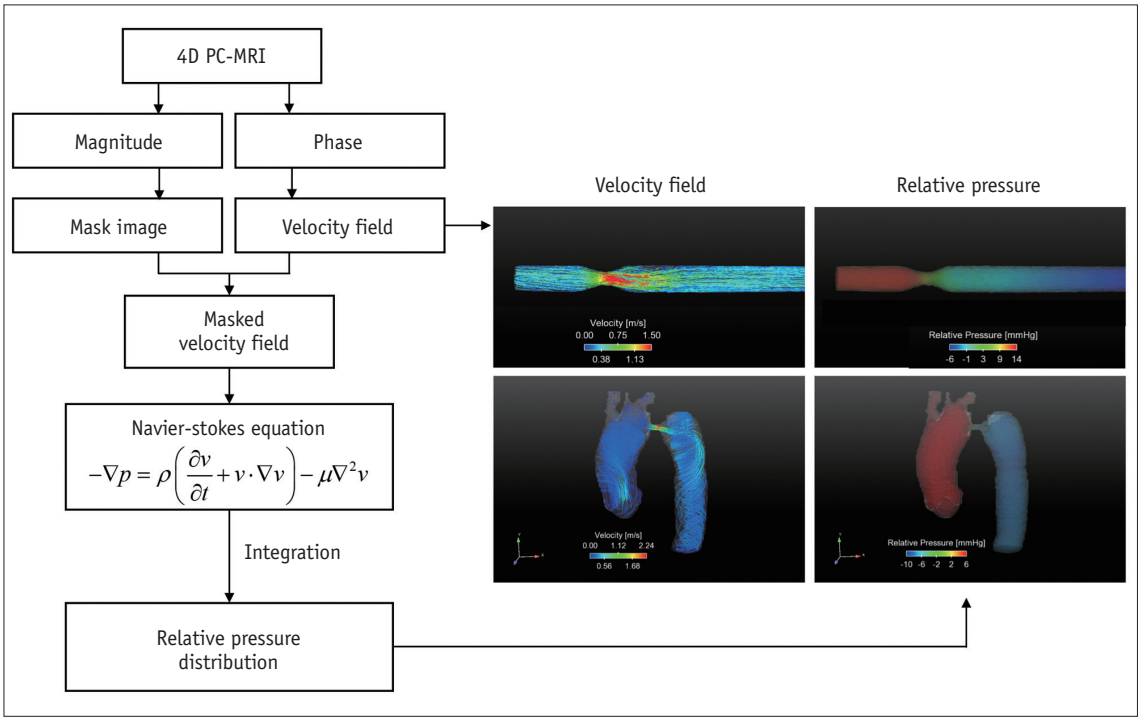

Fig. 7. Procedures for estimation of relative pressure field. Since 4D PC-MRI provides 4D spatio-temporal velocity field, it can be employed to quantify 4D relative pressure distribution along vessel by solving Navier-Stokes equation and reconstructing pressure field over entire vessel of interest. Right panels show representative velocity field and pressure drop through stenotic vessel. PC = phase-contrast, 4D = four-dimensional

Korean Journal of Radiology
KJR

gradient of the pressure can be easily obtained using Eq. (11). Once the pressure gradients over the volumetric regions are obtained, the spatial and temporal variations in the relative pressure field can be obtained by solving the Poisson pressure equation. Notably, the pressure field obtained from Eq. (11) is a relative pressure field without the absolute pressure reference. Therefore, only a pressure gradient can be estimated from the present method without any reference pressure, and the absolute pressure value cannot be obtained.

Clinical Applications

While 3D volumetric acquisition of blood flow using 4D PC-

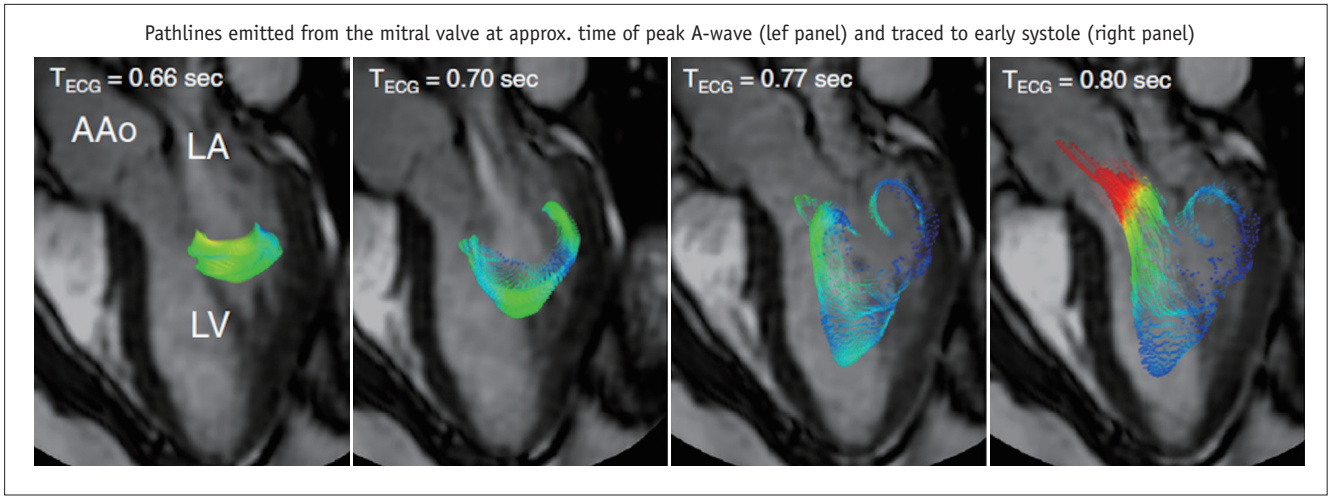

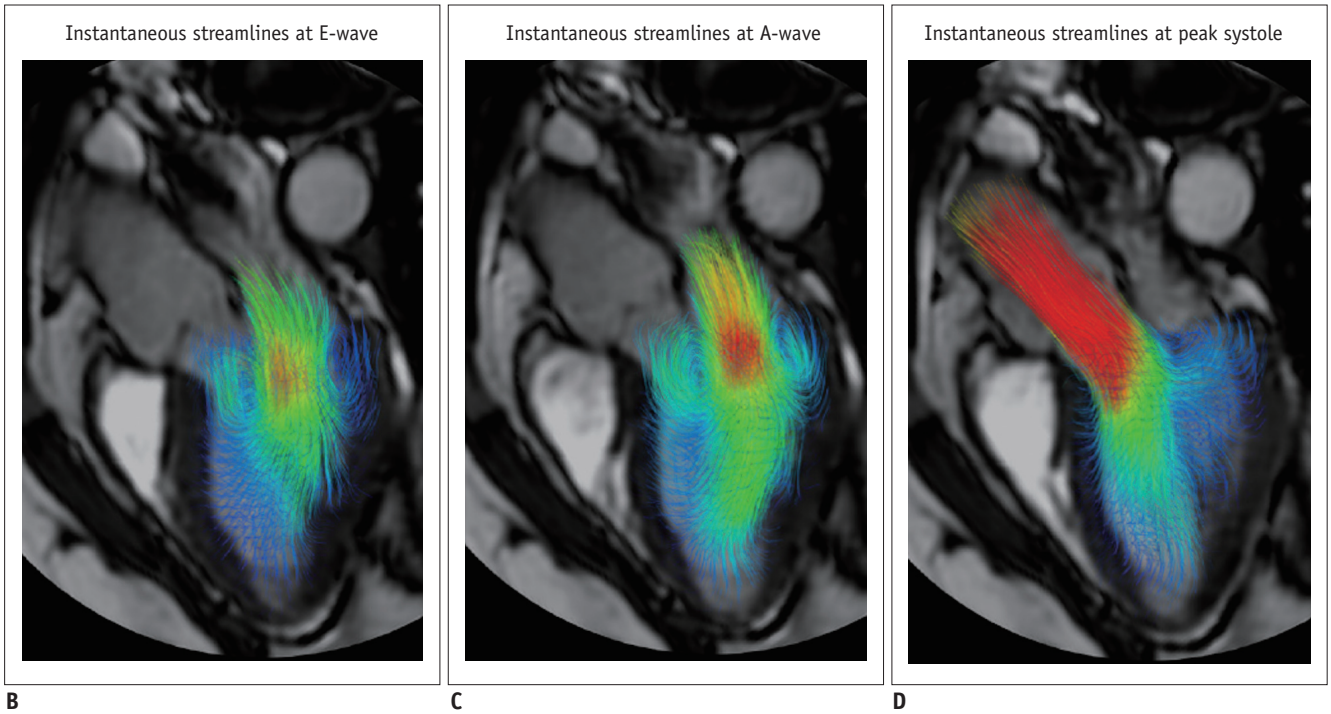

Fig. 8. Examples of 4D flow cardiac magnetic resonance visualization techniques, demonstrated on intracardiac flow data acquired in healthy volunteer. In these examples, flow visualization is overlaid onto 2D bSSFP acquisition in three-chamber view.
A. Pathlines are trajectories that massless fluid particles would follow through dynamic velocity field and are suitable for studies of path of pulsatile blood flow over time. Here, transit of blood through left ventricle (LV) is shown by pathlines emitted from mitral valve at time point of peak A-wave and traced to time point of early systole. Timing of ECG is included for reference. **B-D.** Streamlines are instantaneously tangential to velocity vector field and are useful for visualizing 3D velocity fields at discrete time points. Here, streamlines generated in long-axis plane show parts of intracardiac velocity field at time points of peak early filling (E-wave) **(B)**, peak late filling (A-wave) **(C)**, and peak systole **(D)**. Adapted from Dyverfeldt et al. *J Cardiovasc Magn Reson* 2015;17:72 (30).

MRI takes a long time compared with conventional 2D PC-MRI, it has its own advantages by permitting retrospective investigation of the blood flow for any arbitrary cross-sectional plane within the volumetric data. For this reason, 4D PC-MRI can be useful when multisectional scans of 2D PC-MRI are needed. Previous studies showed that 4D PC-MRI was effective for quantifying the flow rates through various cardiovascular and intracranial arteries and veins with single volumetric acquisition, and the quantification results were comparable with those of conventional 2D PC-MRI (32, 51, 67).

While quantifications of the shunt flow or regurgitation flow using 2D PC-MRI can be inaccurate because the valvular regions move inherently during the cardiac cycle, 4D PC-MRI can consider the motion of the regions of interest. Therefore, 4D PC-MRI can be routinely used as a clinical tool for measuring inlet and outlet valve flow as well as the regurgitation flow through the cardiac valve (14, 68).

In addition, visualization of the time-resolved 3D flow field using 4D PC-MRI enables characterization of the vascular disease-related alteration of blood flow structures by reference to the baseline flow characteristics. Previous studies reported that complex blood flow can be intuitively visualized by describing the transit and accumulation of the blood and the vortical structure identification, and these visualizations were effective for diagnosing the dysfunction of the left ventricles (Fig. 8) (56, 69, 70), the aortic valves (Figs. 9, 10) (4, 71), pulmonary hypertension (Fig. 11) (57), and intracranial blood flow (Fig. 12) (72, 73).

Recently, some multidisciplinary researchers have developed various hemodynamic parameters based on fluid dynamics and demonstrated their clinical implications. WSS is one of the most popular indices for assessing blood flow abnormalities. Recent studies using 4D PC-MRI found that regions of high WSS correspond with extracellular matrix dysregulation and elastic fiber degeneration in the ascending aorta (74). Thus, abnormal WSS might play a major role in the development of aortopathy. Consequently, WSS quantification using 4D PC-MRI could be an important biomarker of disease progression (3, 4, 74). In addition, WSS is suspected to be associated with intracranial aneurysm rupture (75). Therefore, various studies have investigated the feasibility of WSS quantification to predict the risk of intracranial aneurysm (76, 77).

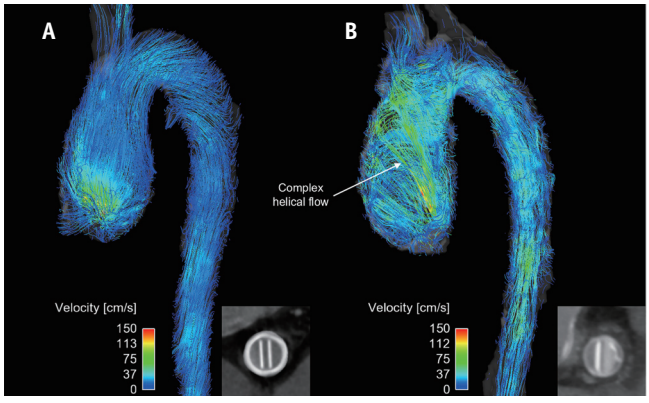

Fig. 10. Comparison of patients with normal (A) and abnormal (B) prosthetic valves. Inset panels indicate opening of prosthetic valves. Note that only abnormal prosthetic valves with partial opening failure generate complex helical blood flow.

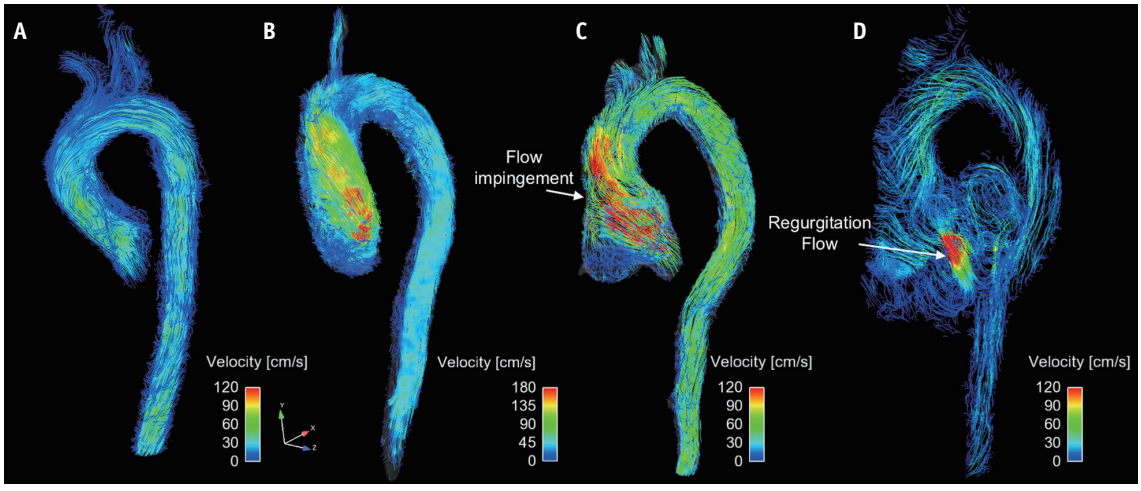

Fig. 9. Visualization of aortic flow.
Normal subject **(A)**, patient with aortic stenosis **(B)**, and patient with aortic regurgitation and aortic root dilatation at systole flow **(C)** and diastole flow **(D)**. Note that aortic flow with aortic stenosis causes helical flow patterns. Aortic flow with aortic dilatation causes impinging flow pattern at systole flow, and substantial amount of regurgitation flow is observed.

Korean Journal of Radiology
KJR

Quantification of TKE using 4D PC-MRI is also a promising biomarker of the efficiency of the blood flow. One study assessed the *in vivo* feasibility of the use of TKE quantification to detect cardiovascular flow abnormalities such as those caused by aortic valve flow and aortic coarctation (18). Recent clinical studies found that patients with dilated cardiomyopathy had higher TKE than healthy subjects (78). In addition, TKE quantification was used as a non-invasive tool for quantifying the severity of aortic stenosis because the TKE value in the ascending aorta was strongly correlated to index pressure loss (Fig. 13) (17).

Non-invasive quantification of the relative pressure using 4D PC-MRI has been mostly developed and validated using aortic flow because the larger vessel guarantees more suitable results (23, 65, 66, 79, 80). Although 4D PC-MRI does not provide the absolute pressure value, it still

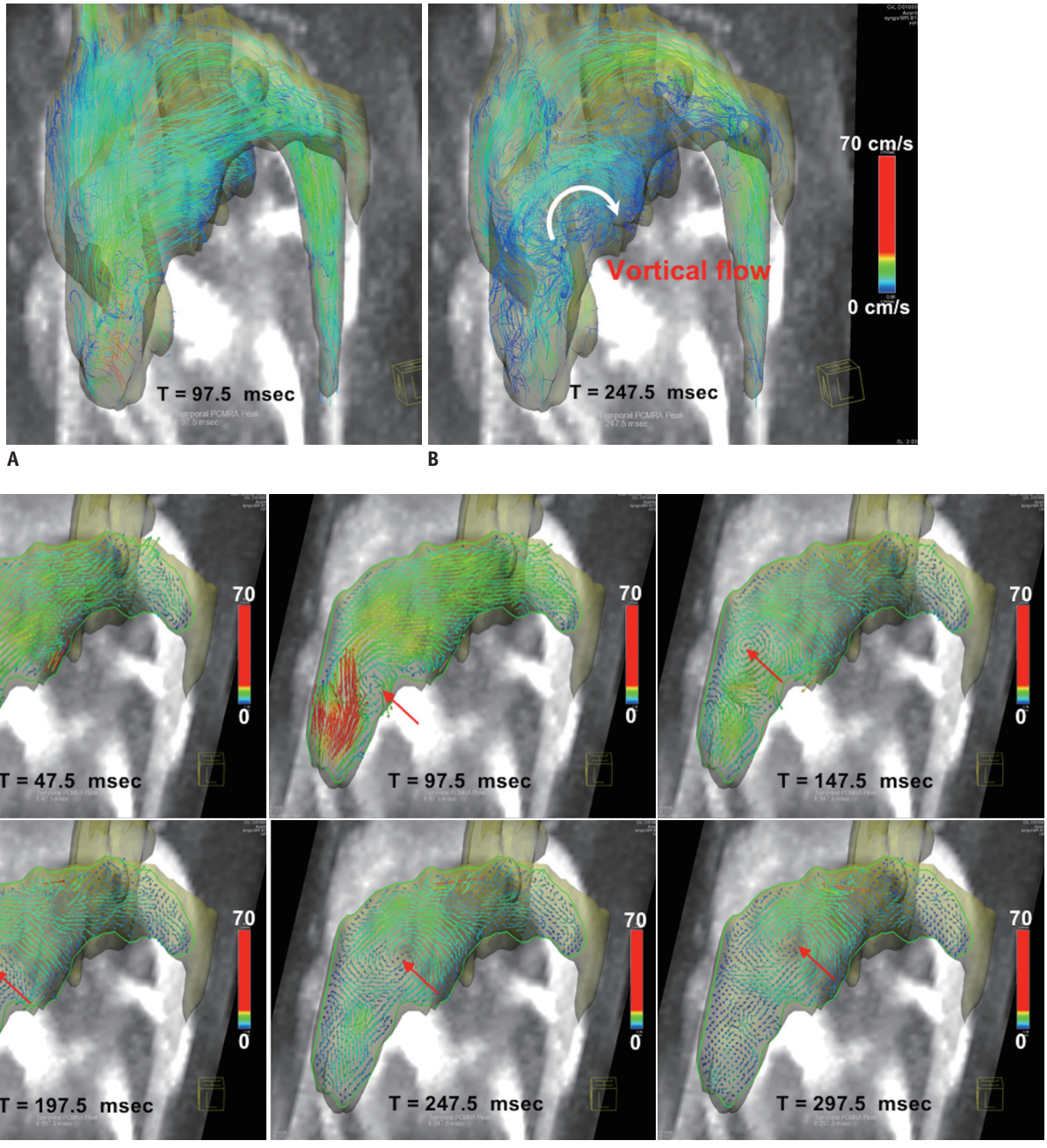

Fig. 11. 4D PC-MRI measurement of patient with pulmonary hypertension.
A, B. Pathline visualization at early systole **(A)** and early diastole **(B)**. **C.** Planar vector visualization of vortical flow pattern. Red arrows indicate center of vortical flow pattern. Note that vortical flow structure at main pulmonary artery appears from early diastole phase. PC = phase-contrast, 4D = four-dimensional

provides the pressure drop information across the aortic coarctation and its temporal variations, such that a time-resolved pressure gradient can be used to assess disease severity (Fig. 13) (65). Non-invasive pressure distributions have also been used to assess carotid, iliac, and renal arteries with stenosis (81, 82). In addition, the pressure field in various types of intra-aneurysms was also validated with invasive microcatheter pressure validation (83). Compared with the point-wise measurement of the catheter-based pressure approach, non-invasive pressure estimation using 4D PC-MRI provides a time-resolved 3D relative pressure field, so that it can identify the relationship between the fluid pattern and the spatial distribution of the dynamic pressure. Consequently, regions with a local peak pressure and spatial deviations could be easily assessed, which cannot be done with invasive catheter pressure measurement (83).

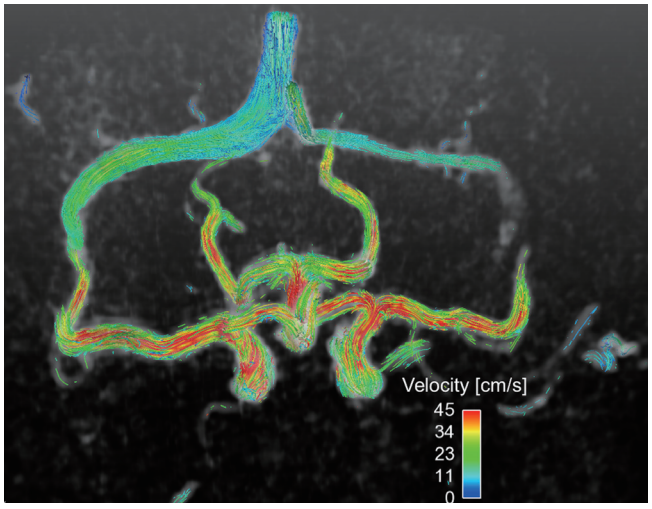

Fig. 12. 4D PC-MRI measurement of intracranial blood flow.
Single volume acquisition using 4D PC-MRI provides volumetric flow distribution in circle of Willis. PC = phase-contrast, 4D = four-dimensional

In addition to the previous quantifications, 4D PC-MRI can also be used to measure pulse wave velocity to assess arterial stiffness and evaluate atherosclerosis progression (24, 84). Pulse wave velocity estimation using 4D PC-MRI acquires volumetric velocity data in the entire aorta and estimates the temporal lag of the blood pulse between the ascending and descending aortas. This parameter was well correlated with the conventional pressure catheter-based estimation and clearly distinguished patients with atherosclerosis from normal controls (24, 84).

While the present article focused on describing quantitative hemodynamic parameters using 4D PC-MRI, it can be noted that many clinical research studies using 4D PC-MRI have also found the utility of qualitative or semi-quantitative analysis of abnormal blood (85, 86). Compared to the normal subjects, the patients with bicuspid aortic valve and aortic stenosis showed frequent helical flow patterns in the ascending aorta (4, 86). In addition, the eccentricity of the aortic flow was also a reliable method for determining the abnormality of the aortic flow (85).

Limitations and Potential

A long scan time is the one of the main limitations of 4D PC-MRI when measuring volumetric regions. Measurement of the major vessels in the head, thorax, and abdomen with a conventional 4D PC-MRI sequence with Cartesian k-space

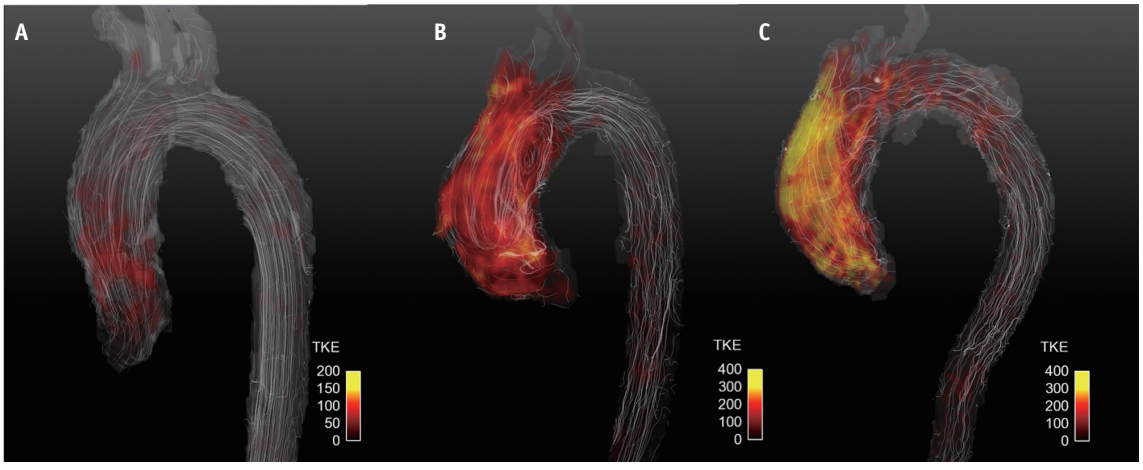

Fig. 13. Turbulent kinetic energy (TKE) estimation using 4D PC-MRI.
Normal subject **(A)**, patient with aortic stenosis with bicuspid aortic valve **(B)**, and patient with aortic stenosis with tricuspid aortic valve **(C)**. Note that patients with aortic stenosis have higher TKE distributions than normal subjects.

Korean Journal of Radiology
KJR

filling takes around 20 minutes when the practical levels of the scan parameters are used (10). The scan time can vary depending on various scan parameters, such as field of view, spatial resolution, temporal resolution, and parallel imaging. Adjusting these parameters to reduce the scan time generally reduces the SNR of the data, which strongly influences the accuracy of the quantifications. Therefore, an appropriate compromise between the scan time and the SNR should be made by considering the objectives of the study. Recently, various new sequences for accelerating the acquisition have been developed, such as k-t undersampling (87), radial sampling (88), and stack-of-stars (89). However, these advanced schemes require further validation before they can be considered suitable for clinical use.

Based on the principle of PC-MRI, each voxel provides the spatially and temporally averaged value of the signal within the voxel (90). Complex blood flow, such as turbulent flow, has a wide range of flow scales, from a few micrometers to a few centimeters, and the temporal spectrum ranges from a few microseconds to a few seconds. Therefore, clinicians and researchers should note that 4D PC-MRI is unable to resolve all blood flow structures, and they need to optimize the spatial and temporal resolutions of 4D PC-MRI by considering the spatiotemporal scales of the flow features of interest.

Although 4D PC-MRI can provide new information to physicians that cannot be found with other imaging modalities, there is no suitable guideline for the use of 4D PC-MRI. A previous guideline for cardiac magnetic resonance could be a useful basis for the future guideline for 4D PC-MRI (91).

The noise of 4D PC-MRI is also one of its limitations. Because the VENC determines the noise level of the velocity field, low-velocity regions are usually less reliable than high-velocity regions due to the overlaid noise. While hemodynamic parameters based on the integration of the velocity field, such as flow rate, are less sensitive to this noise, other estimated parameters based on the derivatives of the velocity field can be significantly influenced by the noise level. Therefore, the influence of the background noise on the quantification of the resultant parameters should be assessed to guarantee the veracity of the results.

For more accurate quantification, pre- or post-processing is vital. Most of these problems depend on the difficulty of image segmentation due to poor image contrast, which could be improved by registration with a separate MR scan, such as balanced steady-state free precession (92) and/or CT angiograms. However, so far, little in-house software has been developed to carry out the segmentation and quantification of 4D flow MRI.

CONCLUSION

Four-dimensional PC-MRI has been improved by the rapid development of sequence, reconstruction, and post-processing techniques. Multidirectional velocity flow measurement with volumetric acquisition enables various retrospective analyses, which might be useful in clinical practice. Multidisciplinary researchers have developed several potential biomarkers based on fluid dynamics, and these biomarkers are being validated in various clinical investigations. While 4D PC-MRI is still being used only for research purposes, it will no doubt soon be available for routine clinical applications as the clinical evidence accumulates.

REFERENCES

1. Fisher AB, Chien S, Barakat AI, Nerem RM. Endothelial cellular response to altered shear stress. *Am J Physiol Lung Cell Mol Physiol* 2001;281:L529-L533
2. Ku DN, Giddens DP, Zarins CK, Glagov S. Pulsatile flow and atherosclerosis in the human carotid bifurcation. Positive correlation between plaque location and low oscillating shear stress. *Arteriosclerosis* 1985;5:293-302
3. Barker AJ, Markl M, Bürk J, Lorenz R, Bock J, Bauer S, et al. Bicuspid aortic valve is associated with altered wall shear stress in the ascending aorta. *Circ Cardiovasc Imaging* 2012;5:457-466
4. Bissell MM, Hess AT, Biasiolli L, Glaze SJ, Loudon M, Pitcher A, et al. Aortic dilation in bicuspid aortic valve disease: flow pattern is a major contributor and differs with valve fusion type. *Circ Cardiovasc Imaging* 2013;6:499-507
5. Uretsky S, Gillam LD. Nature versus nurture in bicuspid aortic valve aortopathy: more evidence that altered hemodynamics may play a role. *Circulation* 2014;129:622-624
6. Slager CJ, Wentzel JJ, Gijsen FJ, Thury A, van der Wal AC, Schaar JA, et al. The role of shear stress in the destabilization of vulnerable plaques and related therapeutic implications. *Nat Clin Pract Cardiovasc Med* 2005;2:456-464
7. Groen HC, Gijsen FJ, van der Lugt A, Ferguson MS, Hatsukami TS, van der Steen AF, et al. Plaque rupture in the carotid artery is localized at the high shear stress region: a case report. *Stroke* 2007;38:2379-2381
8. Markl M, Kilner PJ, Ebbers T. Comprehensive 4D velocity mapping of the heart and great vessels by cardiovascular magnetic resonance. *J Cardiovasc Magn Reson* 2011;13:7
9. Harloff A, Nussbaumer A, Bauer S, Stalder AF, Frydrychowicz A,

Weiller C, et al. In vivo assessment of wall shear stress in the atherosclerotic aorta using flow-sensitive 4D MRI. *Magn Reson Med* 2010;63:1529-1536
10. Markl M, Frydrychowicz A, Kozerke S, Hope M, Wieben O. 4D flow MRI. *J Magn Reson Imaging* 2012;36:1015-1036
11. Morbiducci U, Ponzini R, Rizzo G, Cadioli M, Esposito A, De Cobelli F, et al. In vivo quantification of helical blood flow in human aorta by time-resolved three-dimensional cine phase contrast magnetic resonance imaging. *Ann Biomed Eng* 2009;37:516-531
12. Harloff A, Albrecht F, Spreer J, Stalder AF, Bock J, Frydrychowicz A, et al. 3D blood flow characteristics in the carotid artery bifurcation assessed by flow-sensitive 4D MRI at 3T. *Magn Reson Med* 2009;61:65-74
13. Bammer R, Hope TA, Aksoy M, Alley MT. Time-resolved 3D quantitative flow MRI of the major intracranial vessels: initial experience and comparative evaluation at 1.5T and 3.0T in combination with parallel imaging. *Magn Reson Med* 2007;57:127-140
14. Hsiao A, Tariq U, Alley MT, Lustig M, Vasanawala SS. Inlet and outlet valve flow and regurgitant volume may be directly and reliably quantified with accelerated, volumetric phase-contrast MRI. *J Magn Reson Imaging* 2015;41:376-385
15. Petersson S, Sigfridsson A, Dyverfeldt P, Carlhäll CJ, Ebbers T. Retrospectively gated intracardiac 4D flow MRI using spiral trajectories. *Magn Reson Med* 2016;75:196-206
16. Dyverfeldt P, Gårdhagen R, Sigfridsson A, Karlsson M, Ebbers T. On MRI turbulence quantification. *Magn Reson Imaging* 2009;27:913-922
17. Dyverfeldt P, Hope MD, Tseng EE, Saloner D. Magnetic resonance measurement of turbulent kinetic energy for the estimation of irreversible pressure loss in aortic stenosis. *JACC Cardiovasc Imaging* 2013;6:64-71
18. Dyverfeldt P, Kvitting JP, Sigfridsson A, Engvall J, Bolger AF, Ebbers T. Assessment of fluctuating velocities in disturbed cardiovascular blood flow: in vivo feasibility of generalized phase-contrast MRI. *J Magn Reson Imaging* 2008;28:655-663
19. Kim GB, Ha H, Kweon J, Lee SJ, Kim YH, Yang DH, et al. Post-stenotic plug-like jet with a vortex ring demonstrated by 4D flow MRI. *Magn Reson Imaging* 2016;34:371-375
20. von Spiczak J, Crelier G, Giese D, Kozerke S, Maintz D, Bunck AC. Quantitative analysis of vortical blood flow in the thoracic aorta using 4D phase contrast MRI. *PLoS One* 2015;10:e0139025
21. Donati F, Figueroa CA, Smith NP, Lamata P, Nordsletten DA. Non-invasive pressure difference estimation from PC-MRI using the work-energy equation. *Med Image Anal* 2015;26:159-172
22. Ebbers T, Wigström L, Bolger AF, Engvall J, Karlsson M. Estimation of relative cardiovascular pressures using time-resolved three-dimensional phase contrast MRI. *Magn Reson Med* 2001;45:872-879
23. Krittian SB, Lamata P, Michler C, Nordsletten DA, Bock J, Bradley CP, et al. A finite-element approach to the direct computation of relative cardiovascular pressure from time-resolved MR velocity data. *Med Image Anal* 2012;16:1029-1037
24. Markl M, Wallis W, Brendecke S, Simon J, Frydrychowicz A, Harloff A. Estimation of global aortic pulse wave velocity by flow-sensitive 4D MRI. *Magn Reson Med* 2010;63:1575-1582
25. Markl M, Wallis W, Strecker C, Gladstone BP, Vach W, Harloff A. Analysis of pulse wave velocity in the thoracic aorta by flow-sensitive four-dimensional MRI: reproducibility and correlation with characteristics in patients with aortic atherosclerosis. *J Magn Reson Imaging* 2012;35:1162-1168
26. Pelc NJ, Bernstein MA, Shimakawa A, Glover GH. Encoding strategies for three-direction phase-contrast MR imaging of flow. *J Magn Reson Imaging* 1991;1:405-413
27. Bernstein MA, Ikezaki Y. Comparison of phase-difference and complex-difference processing in phase-contrast MR angiography. *J Magn Reson Imaging* 1991;1:725-729
28. Dumoulin CL, Souza SP, Walker MF, Wagle W. Three-dimensional phase contrast angiography. *Magn Reson Med* 1989;9:139-149
29. Hofman MB, Visser FC, van Rossum AC, Vink QM, Sprenger M, Westerhof N. In vivo validation of magnetic resonance blood volume flow measurements with limited spatial resolution in small vessels. *Magn Reson Med* 1995;33:778-784
30. Dyverfeldt P, Bissell M, Barker AJ, Bolger AF, Carlhäll CJ, Ebbers T, et al. 4D flow cardiovascular magnetic resonance consensus statement. *J Cardiovasc Magn Reson* 2015;17:72
31. Frydrychowicz A, Berger A, Munoz Del Rio A, Russe MF, Bock J, Harloff A, et al. Interdependencies of aortic arch secondary flow patterns, geometry, and age analysed by 4-dimensional phase contrast magnetic resonance imaging at 3 Tesla. *Eur Radiol* 2012;22:1122-1130
32. Meckel S, Leitner L, Bonati LH, Santini F, Schubert T, Stalder AF, et al. Intracranial artery velocity measurement using 4D PC MRI at 3 T: comparison with transcranial ultrasound techniques and 2D PC MRI. *Neuroradiology* 2013;55:389-398
33. Rivera-Rivera LA, Turski P, Johnson KM, Hoffman C, Berman SE, Kilgas P, et al. 4D flow MRI for intracranial hemodynamics assessment in Alzheimer's disease. *J Cereb Blood Flow Metab* 2015 Nov 25 [Epub]. http://dx.doi.org/10.1177/0271678X15617171
34. Schrauben E, Wåhlin A, Ambarki K, Spaak E, Malm J, Wieben O, et al. Fast 4D flow MRI intracranial segmentation and quantification in tortuous arteries. *J Magn Reson Imaging* 2015;42:1458-1464
35. Strecker C, Harloff A, Wallis W, Markl M. Flow-sensitive 4D MRI of the thoracic aorta: comparison of image quality, quantitative flow, and wall parameters at 1.5 T and 3 T. *J Magn Reson Imaging* 2012;36:1097-1103
36. Bernstein MA, Zhou XJ, Polzin JA, King KF, Ganin A, Pelc NJ, et al. Concomitant gradient terms in phase contrast MR: analysis and correction. *Magn Reson Med* 1998;39:300-308
37. Markl M, Bammer R, Alley MT, Elkins CJ, Draney MT, Barnett A, et al. Generalized reconstruction of phase contrast MRI: analysis and correction of the effect of gradient field distortions. *Magn Reson Med* 2003;50:791-801

38. Walker PG, Cranney GB, Scheidegger MB, Waseleski G, Pohost GM, Yoganathan AP. Semiautomated method for noise reduction and background phase error correction in MR phase velocity data. *J Magn Reson Imaging* 1993;3:521-530
39. Abdul-Rahman HS, Gdeisat MA, Burton DR, Lalor MJ, Lilley F, Moore CJ. Fast and robust three-dimensional best path phase unwrapping algorithm. *Appl Opt* 2007;46:6623-6635
40. Chavez S, Xiang QS, An L. Understanding phase maps in MRI: a new cutline phase unwrapping method. *IEEE Trans Med Imaging* 2002;21:966-977
41. Jenkinson M. Fast, automated, N-dimensional phase-unwrapping algorithm. *Magn Reson Med* 2003;49:193-197
42. Salfity MF, Huntley JM, Graves MJ, Marklund O, Cusack R, Beauregard DA. Extending the dynamic range of phase contrast magnetic resonance velocity imaging using advanced higher-dimensional phase unwrapping algorithms. *J R Soc Interface* 2006;3:415-427
43. Salfity MF, Ruiz PD, Huntley JM, Graves MJ, Cusack R, Beauregard DA. Branch cut surface placement for unwrapping of undersampled three-dimensional phase data: application to magnetic resonance imaging arterial flow mapping. *Appl Opt* 2006;45:2711-2722
44. Szumowski J, Coshow WR, Li F, Quinn SF. Phase unwrapping in the three-point Dixon method for fat suppression MR imaging. *Radiology* 1994;192:555-561
45. Bustamante M, Petersson S, Eriksson J, Alehagen U, Dyverfeldt P, Carlhäll CJ, et al. Atlas-based analysis of 4D flow CMR: automated vessel segmentation and flow quantification. *J Cardiovasc Magn Reson* 2015;17:87
46. van Pelt R, Oliván Bescós J, Breeuwer M, Clough RE, Gröller ME, ter Haar Romenij B, et al. Exploration of 4D MRI blood flow using stylistic visualization. *IEEE Trans Vis Comput Graph* 2010;16:1339-1347
47. van Pelt R, Nguyen H, ter Haar Romeny B, Vilanova A. Automated segmentation of blood-flow regions in large thoracic arteries using 3D-cine PC-MRI measurements. *Int J Comput Assist Radiol Surg* 2012;7:217-224
48. Bagan P, Vidal R, Martinod E, Destable MD, Tremblay B, Dumas JL, et al. Cerebral ischemia during carotid artery cross-clamping: predictive value of phase-contrast magnetic resonance imaging. *Ann Vasc Surg* 2006;20:747-752
49. Hope TA, Hope MD, Purcell DD, von Morze C, Vigneron DB, Alley MT, et al. Evaluation of intracranial stenoses and aneurysms with accelerated 4D flow. *Magn Reson Imaging* 2010;28:41-46
50. Garcia J, Barker AJ, van Ooij P, Schnell S, Puthumana J, Bonow RO, et al. Assessment of altered three-dimensional blood characteristics in aortic disease by velocity distribution analysis. *Magn Reson Med* 2015;74:817-825
51. Markl M, Chan FP, Alley MT, Wedding KL, Draney MT, Elkins CJ, et al. Time-resolved three-dimensional phase-contrast MRI. *J Magn Reson Imaging* 2003;17:499-506
52. Stalder AF, Russe MF, Frydrychowicz A, Bock J, Hennig J, Markl M. Quantitative 2D and 3D phase contrast MRI: optimized analysis of blood flow and vessel wall parameters. *Magn Reson Med* 2008;60:1218-1231
53. Mathieu J, Scott J. An introduction to turbulent flow. Cambridge: Cambridge University Press, 2000:10-11
54. Dyverfeldt P, Sigfridsson A, Kvitting JP, Ebbers T. Quantification of intravoxel velocity standard deviation and turbulence intensity by generalizing phase-contrast MRI. *Magn Reson Med* 2006;56:850-858
55. Wong KK, Kelso RM, Worthley SG, Sanders P, Mazumdar J, Abbott D. Cardiac flow analysis applied to phase contrast magnetic resonance imaging of the heart. *Ann Biomed Eng* 2009;37:1495-1515
56. Elbaz MS, Calkoen EE, Westenberg JJ, Lelieveldt BP, Roest AA, van der Geest RJ. Vortex flow during early and late left ventricular filling in normal subjects: quantitative characterization using retrospectively-gated 4D flow cardiovascular magnetic resonance and three-dimensional vortex core analysis. *J Cardiovasc Magn Reson* 2014;16:78
57. Reiter G, Reiter U, Kovacs G, Olschewski H, Fuchsjäger M. Blood flow vortices along the main pulmonary artery measured with MR imaging for diagnosis of pulmonary hypertension. *Radiology* 2015;275:71-79
58. Jeong J, Hussain F. On the identification of a vortex. *J Fluid Mech* 1995;285:69-94
59. Zhou J, Adrian RJ, Balachandar S. Autogeneration of near-wall vortical structures in channel flow. *Phys Fluids* 1996;8:288-290
60. Zhou J, Adrian RJ, Balachandar S, Kendall TM. Mechanisms for generating coherent packets of hairpin vortices in channel flow. *J Fluid Mech* 1999;387:353-396
61. Adrian RJ, Christensen KT, Liu ZC. Analysis and interpretation of instantaneous turbulent velocity fields. *Exp Fluids* 2000;29:275-290
62. Currie PJ, Seward JB, Reeder GS, Vlietstra RE, Bresnahan DR, Bresnahan JF, et al. Continuous-wave Doppler echocardiographic assessment of severity of calcific aortic stenosis: a simultaneous Doppler-catheter correlative study in 100 adult patients. *Circulation* 1985;71:1162-1169
63. Cohn JN, Quyyumi AA, Hollenberg NK, Jamerson KA. Surrogate markers for cardiovascular disease: functional markers. *Circulation* 2004;109(25 Suppl 1):IV31-IV46
64. Stamm RB, Martin RP. Quantification of pressure gradients across stenotic valves by Doppler ultrasound. *J Am Coll Cardiol* 1983;2:707-718
65. Bock J, Frydrychowicz A, Lorenz R, Hirtler D, Barker AJ, Johnson KM, et al. In vivo noninvasive 4D pressure difference mapping in the human aorta: phantom comparison and application in healthy volunteers and patients. *Magn Reson Med* 2011;66:1079-1088
66. Ebbers T, Farnebäck G. Improving computation of cardiovascular relative pressure fields from velocity MRI. *J Magn Reson Imaging* 2009;30:54-61
67. Hope MD, Meadows AK, Hope TA, Ordovas KG, Saloner D, Reddy GP, et al. Clinical evaluation of aortic coarctation with 4D flow MR imaging. *J Magn Reson Imaging* 2010;31:711-718
68. Roes SD, Hammer S, van der Geest RJ, Marsan NA, Bax JJ,

Lamb HJ, et al. Flow assessment through four heart valves simultaneously using 3-dimensional 3-directional velocity-encoded magnetic resonance imaging with retrospective valve tracking in healthy volunteers and patients with valvular regurgitation. *Invest Radiol* 2009;44:669-675
69. Eriksson J, Bolger AF, Ebbers T, Carlhäll CJ. Four-dimensional blood flow-specific markers of LV dysfunction in dilated cardiomyopathy. *Eur Heart J Cardiovasc Imaging* 2013;14:417-424
70. Calkoen EE, Roest AA, Kroft LJ, van der Geest RJ, Jongbloed MR, van den Boogaard PJ, et al. Characterization and improved quantification of left ventricular inflow using streamline visualization with 4DFlow MRI in healthy controls and patients after atrioventricular septal defect correction. *J Magn Reson Imaging* 2015;41:1512-1520
71. Hope MD, Hope TA, Crook SE, Ordovas KG, Urbania TH, Alley MT, et al. 4D flow CMR in assessment of valve-related ascending aortic disease. *JACC Cardiovasc Imaging* 2011;4:781-787
72. Berg P, Stucht D, Janiga G, Beuing O, Speck O, Thévenin D. Cerebral blood flow in a healthy Circle of Willis and two intracranial aneurysms: computational fluid dynamics versus four-dimensional phase-contrast magnetic resonance imaging. *J Biomech Eng* 2014;136:041003
73. Schnell S, Ansari SA, Vakil P, Wasielewski M, Carr ML, Hurley MC, et al. Three-dimensional hemodynamics in intracranial aneurysms: influence of size and morphology. *J Magn Reson Imaging* 2014;39:120-131
74. Guzzardi DG, Barker AJ, van Ooij P, Malaisrie SC, Puthumana JJ, Belke DD, et al. Valve-related hemodynamics mediate human bicuspid aortopathy: insights from wall shear stress mapping. *J Am Coll Cardiol* 2015;66:892-900
75. Jou LD, Lee DH, Morsi H, Mawad ME. Wall shear stress on ruptured and unruptured intracranial aneurysms at the internal carotid artery. *AJNR Am J Neuroradiol* 2008;29:1761-1767
76. van Ooij P, Potters WV, Guédon A, Schneiders JJ, Marquering HA, Majoie CB, et al. Wall shear stress estimated with phase contrast MRI in an in vitro and in vivo intracranial aneurysm. *J Magn Reson Imaging* 2013;38:876-884
77. Isoda H, Ohkura Y, Kosugi T, Hirano M, Takeda H, Hiramatsu H, et al. In vivo hemodynamic analysis of intracranial aneurysms obtained by magnetic resonance fluid dynamics (MRFD) based on time-resolved three-dimensional phase-contrast MRI. *Neuroradiology* 2010;52:921-928
78. Zajac J, Eriksson J, Dyverfeldt P, Bolger AF, Ebbers T, Carlhäll CJ. Turbulent kinetic energy in normal and myopathic left ventricles. *J Magn Reson Imaging* 2015;41:1021-1029
79. Tyszka JM, Laidlaw DH, Asa JW, Silverman JM. Three-dimensional, time-resolved (4D) relative pressure mapping using magnetic resonance imaging. *J Magn Reson Imaging* 2000;12:321-329
80. Yang GZ, Kilner PJ, Wood NB, Underwood SR, Firmin DN. Computation of flow pressure fields from magnetic resonance velocity mapping. *Magn Reson Med* 1996;36:520-526
81. Bley TA, Johnson KM, François CJ, Reeder SB, Schiebler ML, R Landgraf B, et al. Noninvasive assessment of transstenotic pressure gradients in porcine renal artery stenoses by using vastly undersampled phase-contrast MR angiography. *Radiology* 2011;261:266-273
82. Lum DP, Johnson KM, Paul RK, Turk AS, Consigny DW, Grinde JR, et al. Transstenotic pressure gradients: measurement in swine--retrospectively ECG-gated 3D phase-contrast MR angiography versus endovascular pressure-sensing guidewires. *Radiology* 2007;245:751-760
83. Moftakhar R, Aagaard-Kienitz B, Johnson K, Turski PA, Turk AS, Niemann DB, et al. Noninvasive measurement of intra-aneurysmal pressure and flow pattern using phase contrast with vastly undersampled isotropic projection imaging. *AJNR Am J Neuroradiol* 2007;28:1710-1714
84. Wentland AL, Wieben O, François CJ, Boncyk C, Munoz Del Rio A, Johnson KM, et al. Aortic pulse wave velocity measurements with undersampled 4D flow-sensitive MRI: comparison with 2D and algorithm determination. *J Magn Reson Imaging* 2013;37:853-859
85. Sigovan M, Hope MD, Dyverfeldt P, Saloner D. Comparison of four-dimensional flow parameters for quantification of flow eccentricity in the ascending aorta. *J Magn Reson Imaging* 2011;34:1226-1230
86. Manka R, Busch J, Crelier G, Lüscher TF, Kozerke S. Pre- and post-operative assessment of valvular and aortic flow using 4D flow magnetic resonance imaging. *Eur Heart J* 2013;34:1423
87. Schnell S, Markl M, Entezari P, Mahadewia RJ, Semaan E, Stankovic Z, et al. k-t GRAPPA accelerated four-dimensional flow MRI in the aorta: effect on scan time, image quality, and quantification of flow and wall shear stress. *Magn Reson Med* 2014;72:522-533
88. Johnson KM, Lum DP, Turski PA, Block WF, Mistretta CA, Wieben O. Improved 3D phase contrast MRI with off-resonance corrected dual echo VIPR. *Magn Reson Med* 2008;60:1329-1336
89. Kecskemeti S, Johnson K, Wu Y, Mistretta C, Turski P, Wieben O. High resolution three-dimensional cine phase contrast MRI of small intracranial aneurysms using a stack of stars k-space trajectory. *J Magn Reson Imaging* 2012;35:518-527
90. Petersson S, Dyverfeldt P, Gårdhagen R, Karlsson M, Ebbers T. Simulation of phase contrast MRI of turbulent flow. *Magn Reson Med* 2010;64:1039-1046
91. Yoon YE, Hong YJ, Kim HK, Kim JA, Na JO, Yang DH, et al. 2014 Korean guidelines for appropriate utilization of cardiovascular magnetic resonance imaging: a joint report of the Korean Society of Cardiology and the Korean Society of Radiology. *Korean J Radiol* 2014;15:659-688
92. Park SH, Han PK, Choi SH. Physiological and functional magnetic resonance imaging using balanced steady-state free precession. *Korean J Radiol* 2015;16:550-559